Nanocrystals Hot Paper

Deutsche Ausgabe: DOI: 10.1002/ange.201701321
Internationale Ausgabe: DOI: 10.1002/anie.201701321

Size-Tunable Photothermal Germanium Nanocrystals

Wei Sun[+], Grace Zhong[+], Christian Kübel, Abdinoor A. Jelle, Chenxi Qian, Lu Wang, Manuchehr Ebrahimi, Laura M. Reyes, Amr S. Helmy, and Geoffrey A. Ozin**

Abstract: *Germanium nanocrystals (ncGe) have not received as much attention as silicon nanocrystals (ncSi). However, Ge has demonstrated superiority over Si nanomaterials in some applications. Examples include, high charge–discharge rate lithium-ion batteries,[1] small band-gap opto-electronic devices,[2] and photo-therapeutics.[3] When stabilized in an oxide matrix (ncGe/GeO_x), its high charge-retention has enabled non-volatile memories.[4] It has also found utility as a high-capacity anode material for Li-ion batteries with impressive stability.[5] Herein, we report an organic-free synthesis of size-controlled ncGe in a GeO_x matrix as well as freestanding ncGe, via the thermal disproportionation of GeO prepared from thermally induced dehydration of $Ge(OH)_2$. The photothermal effect of ncGe, quantified by Raman spectroscopy, is found to be size dependent and superior to ncSi. This advance suggests applications of ncGe in photothermal therapy, desalination, and catalysis.*

Reported methods for making ncGe include: gas-phase plasma synthesis,[6] solution-phase synthesis using Zintl salts,[7] or via reduction of germanium ions,[8] solid–liquid laser ablation,[2a] and solid-phase synthesis using organogermanium polymers.[9] Thermal batch processing of polymeric solid $(C_6H_5GeO_{1.5})_n$ allows for control of the ncGe size embedded in the matrix through control over the processing temperature,[10] work inspired by the synthesis of ncSi using hydrogen silsesquioxane ($Si_8O_{12}H_8$) or $(HSiO_{1.5})_n(CH_3SiO_{1.5})_m$ as the precursor.[11] In the case of germanium, like silicon, the thermally processed polymers disproportionate to Ge^0 and Ge^{IV}. However, the organogermanium polymer precursors suffer from the problem of inescapable carbon contamination of the resulting ncGe,[10] so an all-inorganic precursor, such as GeO is a desirable and sought after alternative.

We have reported that thermal processing of the organic-free precursor SiO is a straightforward, scalable, and convenient approach for producing size-controlled ncSi. This synthetic pathway to ncSi offered the advantages of requiring lower processing temperatures, producing higher yields with higher atomic efficiency, and providing a wider range of sizes.[12]

This advance in silicon nanochemistry has inspired the work described herein, which explores for the first time, the use of GeO as a precursor for the synthesis of size-controlled ncGe embedded in a GeO_x matrix as well as free-standing ncGe, by straightforward etching of the matrix. The thermal disproportionation of GeO is probed in detail by diffraction, microscopy, and spectroscopy. The intense absorption of light throughout the entire solar spectral wavelength range and the impressive photothermal effect discovered for ncGe, bodes well for applications in photocatalysis, phototherapy, and photodesalination, offering possible solutions to some of the most urgent environmental and health problems.

GeO has an interesting and curious history. Unlike SiO it is rarely available commercially. It was reported to be formed by co-condensing the vapors of Ge and GeO_2 at high temperatures and under vacuum.[13] Forty years ago it was reported that GeO can be obtained by dehydration of germanium(II) hydroxide [Eq. (1)]:[14]

$$Ge(OH)_2 \rightarrow GeO + H_2O \quad (1)$$

Encouraged by this report we developed a synthesis of GeO that uses freshly prepared $Ge(OH)_2{\cdot}x\,H_2O$, made from low-cost GeO_2 powder, using hypophosphorous acid (H_3PO_2) as a mild reducing agent [Eq. (2)]:[15]

$$Ge^{IV} + H_2O + H_3PO_2 \rightarrow H_3PO_3 + Ge^{II} + 2H^+ \quad (2)$$

In this reaction, the Ge^{IV} was selectively reduced to Ge^{II} which was then precipitated from aqueous solution by addition of weak base.[16] The detailed experimental procedure can be found in the supporting information.

Thermogravimetric analysis (TGA) of $Ge(OH)_2{\cdot}x\,H_2O$ dried under vacuum confirms that significant weight loss occurred below 300 °C (Figure S1 in the Supporting Information), suggesting loss of water. This solid-state reaction can be directly evidenced by IR spectroscopy. In Figure 1, the bands in the OH region of $Ge(OH)_2{\cdot}x\,H_2O$ between 2500 and 3750 cm^{-1} became barely observable after being processed at 300 °C for 2 h or above in 5 % H_2/95 % Ar gas. The latter is the

[*] Dr. W. Sun,[+] C. Qian, Dr. L. Wang, L. M. Reyes, Prof. G. A. Ozin
Department of Chemistry, University of Toronto
80 St. George Street, Toronto, Ontario M5S 3H6 (Canada)
E-mail: gozin@chem.utoronto.ca

G. Zhong,[+] M. Ebrahimi, Prof. A. S. Helmy
The Edward S. Rogers Sr. Department of Electrical and Computer Engineering, University of Toronto
10 King's College Road, Toronto, Ontario M5S 3G4 (Canada)
E-mail: a.helmy@utoronto.ca

Dr. C. Kübel
Institute of Nanotechnology (INT) and Karlsruhe Nano Micro Facility (KNMF), Karlsruhe Institute of Technology (KIT)
Hermann-von-Helmholtz Platz 1
76344 Eggenstein-Leopoldshafen (Germany)

A. A. Jelle
Department of Materials Science and Engineering
University of Toronto
184 College Street, Toronto, Ontario M5S 3E4 (Canada)

[+] These authors contributed equally to this work.

Supporting information and the ORCID identification number(s) for the author(s) of this article can be found under: https://doi.org/10.1002/anie.201701321.

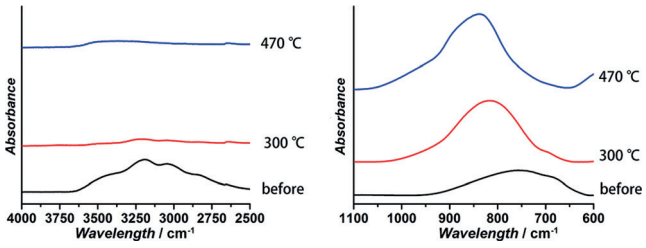

Figure 1. Sections of the ATR-FTIR spectra of the $Ge(OH)_2{\cdot}x\,H_2O$ powder before thermal processing, after 300 °C processing for 2 h, and after processing at 300 °C for 2 h and subsequently at 470 °C for 1 h.

most commonly used atmosphere for enhancing both the yield and enabling the size tuning for this kind of nanocrystal solid state synthesis.[17]

The freshly prepared $Ge(OH)_2{\cdot}x\,H_2O$ powder after vacuum treatment at 100 °C overnight appeared amorphous initially before any further thermal processing, seen in the X-ray powder diffraction (XRD) pattern in Figure 2. Even

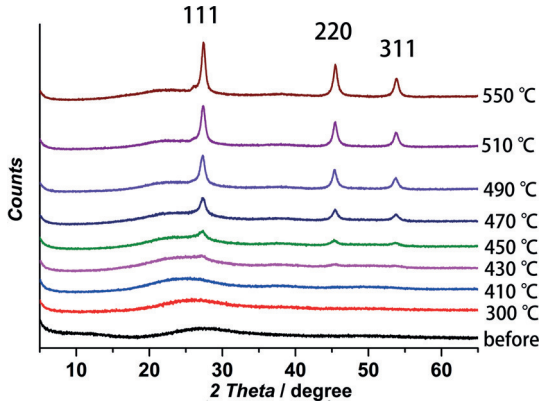

Figure 2. XRD patterns of the $Ge(OH)_2{\cdot}x\,H_2O$ powder processed at various temperatures.

after dehydration at 300 °C for 2 h, still no crystalline Ge was detected. Amorphous small clusters of Ge might exist at this stage resembling the situation in SiO,[18] but they lack long-range crystalline order. This implies the production of ncGe originates mainly from the thermally induced disproportionation and crystallization reaction that occurs at higher temperatures [Eq. (3)]:[19]

$$2\,GeO \rightarrow Ge + GeO_2 \qquad (3)$$

As seen in Figure 2, as the processing temperature was elevated, starting from 430 °C, the emergence of the (111) diffraction peaks of ncGe occurred, defining the formation of embryonic ncGe. However, only above 470 °C are the (220) and (311) diffraction peaks of ncGe clearly observable above the background, indicating increasing amounts of ncGe were being produced. The gradual shift of the broad amorphous matrix diffraction hump from approximately 27.5 degrees to around 23 degrees also probes the transformation of the matrix towards a GeO_2 like structure upon disproportionation. This is consistent with the IR result in Figure 1 that the Ge–O region originally centered at 750 cm^{-1} also shifted towards larger wavenumbers upon heating, reaching about 860 cm^{-1} after 470 °C processing, closer to the value of GeO_2 glass, at 916 cm^{-1},[20] indicating the matrix structure begins to approach that of GeO_2.

To quantitatively show that the ncGe size and yield could be tuned by control of the processing temperature, we have performed Rietveld refinement of the PXRD patterns (fitting details in the Supporting Information). The results in Table 1

Table 1: Ge size, Ge crystalline wt%, and amorphous phase wt% of samples processed at different temperatures, determined by XRD.

Sample	Size [nm][a]	Crystalline wt%	Amorphous wt%
410	N/A	N/A	100
430	5 (2)	14	86
450	13 (3)	21.2	79.8
470	16 (4)	35.1	64.9
490	18 (4)	52.3	47.6
510	25 (5)	60.5	39.5
550	30 (7)	59.4	40.6

[a] The values in parentheses are estimated standard deviations (ESD). At low temperatures (430, 450 °C) the ncGe peaks are quite broad and their size shows significant ESDs in consecutive refinements. The mean values were considered.

clearly shows that the size monotonically increases with processing temperature, accompanied by a corresponding increase of crystalline fraction as compared to the amorphous matrix. Above 470 °C the refinement improved in quality due to the better clarity of the peak shapes. The crystalline fraction seems to have reached a plateau at around 510 °C, though the ncGe size keeps increasing. The trend of increasing size and yield of ncGe versus processing temperature is expected since the disproportionation generates Ge^0 which increasingly accretes Ge^0 in the matrix, consistent with the observation that Ge starts to slowly crystallize at 475 °C.[21] The slightly reducing atmosphere serves to enhance the yield of ncGe at these higher temperatures.[17]

Direct evidence of the proposed disproportionation was also captured by X-ray photoelectron spectroscopy (XPS). The sample processed at 300 °C, which contains no detectable ncGe by PXRD, shows only one peak at the Ge 3d region assigned to Ge^{II} in the form of GeO (Figure 3). On processing at 470 °C the single Ge^{II} peak divides into two, straddled on both its sides by peaks that can be assigned to Ge^{IV} with the higher binding energy and Ge^0 with the lower binding energy (Figure 3), indicating the formation of GeO_2 and ncGe, respectively.

With the increase of the crystalline Ge fraction and the change of the matrix structure from GeO to Ge and GeO_2, we also observed an accompanying gradual change of color of the samples, from brown to black with the increase of the processing temperature (Figure S2). The dark color indicates significant broad-band, light absorption throughout the solar spectral wavelength range, as shown in Figure 4, for samples heated between 430 °C and 550 °C. They all exhibit less than 30% reflectance in the visible range, and below 10%

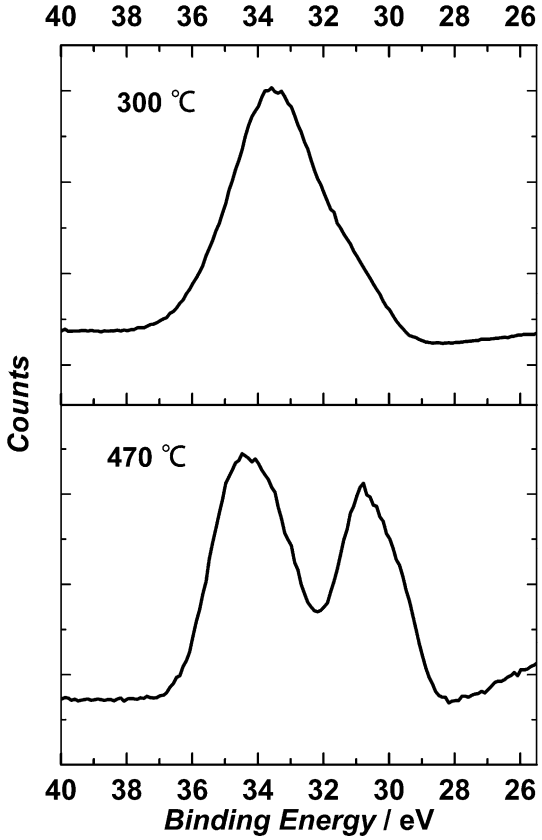

Figure 3. XPS patterns of the Ge 3d regions of the samples processed at 300 °C and 470 °C.

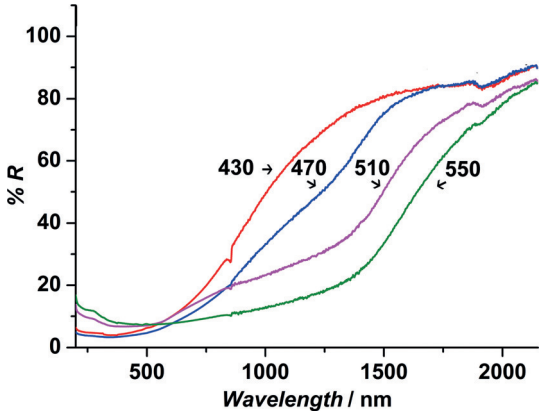

Figure 4. UV/Vis spectra in % R mode of GeO processed at increasing temperatures.

reflectance in the ultraviolet range. Notably, they begin to show differences in the near-infrared range at wavelengths longer than 800 nm. This corresponds with the growth of ncGe, which with increasing size absorb longer wavelength light originating from the quantum confinement effect.

In what follows we turn attention to Raman Spectroscopy of ncGe as a probe of phonon confinement[12a] and associated photothermal effects.[22] As seen in Figure 5, all thermally processed GeO samples display multiple Raman peaks excited by a 784 nm laser light source, the assignment of

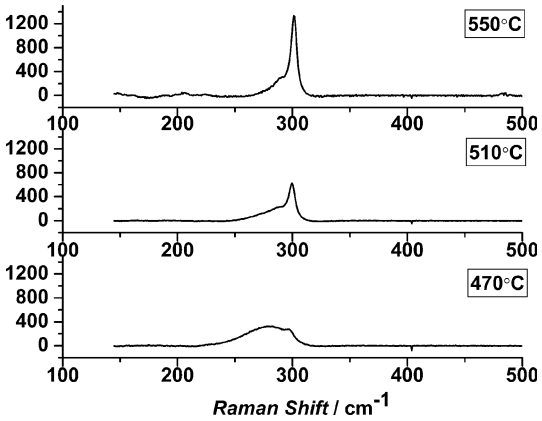

Figure 5. Raman spectra of GeO samples processed at 470 °C, 510 °C, and 550 °C, showing increasingly sharp ncGe signals coexisting with amorphous Ge broad signals.

which are shown in Figure S3. From the observable differences in the area of the amorphous Ge peak at around 275 cm^{-1} in Figure 5, it is clear that higher processing temperatures led to a higher crystalline fraction of ncGe.

The crystallinity (X_c) is calculated using the Equation (4) where S_l, S_s, and S_a are Raman peak areas corresponding to large ncGe at approximately 300 cm^{-1}, small ncGe at around 290 cm^{-1}, and amorphous Ge at about 275 cm^{-1}, respectively.[23] The Raman scattering cross section ratio σ is determined by the Equation (5)

$$X_c = \frac{S_l + S_s}{(S_l + S_s) + S_a\sigma} \tag{4}$$

$$\sigma(L) = 0.1 + \exp\left(-\frac{L}{250}\right)\exp\left(\frac{-h\nu_k}{kT}\right) = \left(\frac{\sigma[\alpha_{\nu_k}]_s}{\sigma[\alpha_{\nu_k}]_a}\right)\left(\frac{I_a[\nu_k]}{I_s[\nu_k]}\right)\left(\frac{\nu_o - \nu_k}{\nu_o + \nu_k}\right)^4 \tag{5}$$

where L is the mean ncGe diameter in angstrom determined by PXRD.[24] The crystalline fractions for each sample are shown in Table 2. Independent of the laser power applied, the crystalline fraction results display very good consistency within each sample processed at a certain temperature, confirming the accuracy of the measurements. Between samples processed at different temperatures, there are large differences in crystalline fraction, especially between the samples processed at 470 °C (the threshold temperature for significant generation and crystallization of ncGe discussed above) and at 510 °C, and thermal processing at 550 °C led to a steady-state defining the point of complete disappearance of the amorphous Ge mode at approximately 275 cm^{-1}, indicating essentially complete crystallization of ncGe.

Table 2: Crystalline fraction for different processing temperatures used during synthesis, calculated using Raman spectra obtained with different laser powers.

Sample	0.035 mW	0.35 mW	3.5 mW
470 °C	0.35	0.40	0.39
510 °C	0.85	0.80	0.78
550 °C	1	1	1

To explore the photothermal effect of the GeO samples, we explored the impact of excitation laser power on the Raman spectra. As expected, we observed a down-shift of the main ncGe Raman mode for all samples as the laser power increased in Figure 6, which is typically associated with

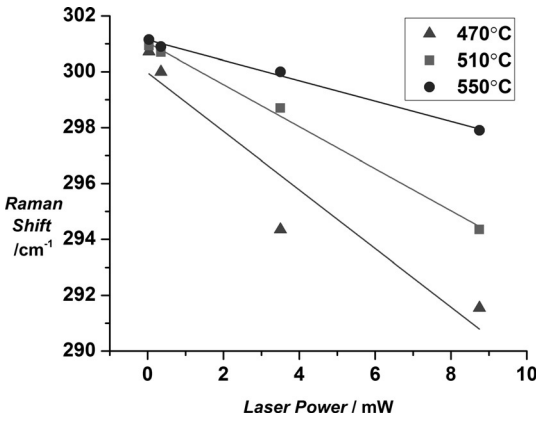

Figure 6. ncGe Raman shift position of the GeO samples processed at 470 °C, 510 °C, and 550 °C, excited at different laser power levels.

a photothermal phenomenon, similarly found in ncSi.[25] In such a nanostructure the heat could not dissipate efficiently as in the bulk. At the lowest power applied, the 470 °C processed samples already have the smallest Raman shift, attributed to the strongest phonon confinement effect[26] since their crystal sizes are the smallest. The down-shifting tendency of the 470 °C processed samples are also more significant than the samples processed at higher temperatures, which indicates a more sensitive heating effect with the increasing power level applied. The peak position of the 470 °C processed sample obtained at the highest power applied seems also deviated from the trend formed by the other three points, also suggesting the significant heating effect might have increased the ncGe size through thermal crystallization. These heating effects were probed through a study of the Stokes and *anti*-Stokes Raman modes of ncGe by estimation of the local temperature via Equation (6)

$$\exp\left(\frac{-h\nu_k}{kT}\right) = \left(\frac{\sigma[\alpha_{\nu_k}]_s}{\sigma[\alpha_{\nu_k}]_a}\right)\left(\frac{I_a[\nu_k]}{I_s[\nu_k]}\right)\left(\frac{\nu_o-\nu_k}{\nu_o+\nu_k}\right)^4 \quad \text{Ref. [27]} \qquad (6)$$

where $\sigma[\alpha_{vk}]_s$ and $\sigma[\alpha_{vk}]_a$ are Stokes and *anti*-Stokes Raman cross sections, which are related to the polarizability at the scattering mode of interest.[27b] The factor $\sigma[\alpha_{vk}]_s/\sigma[\alpha_{vk}]_a$ was estimated for each sample by assuming a local temperature of 300 K for all samples at the lowest laser power (Supporting Information).[28]

To establish the reliability of such an estimation of local temperature of laser excited semiconductor nanocrystals, we applied the same measurement conditions to SiO samples produced similarly.[12b] From Figure 7, for both GeO and SiO, as the processing temperature decreased, we observed an increase in local temperature with increasing laser power. Notably, we observed a significantly larger increase in

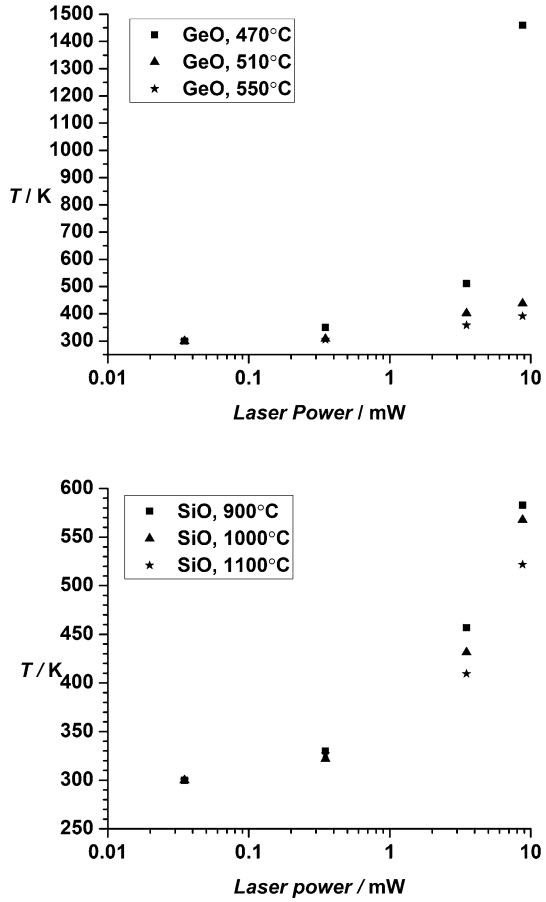

Figure 7. Estimated temperatures at different incident laser powers for, top: GeO samples, bottom: SiO samples, thermally processed at the indicated temperatures.

temperature for GeO processed at 470 °C as compared to GeO processed at 510 °C and 550 °C. At the highest laser power of 8.75 mW (corresponding with a power density of 984 kW cm^{-2}, estimated from the laser spot size), the temperature of the 470 °C processed sample is estimated to be 1460 K, while the temperature for the 510 °C and 550 °C processed samples are estimated to be 438 K and 392 K respectively. The thermally processed SiO samples have a smaller difference in the local temperature with increasing power but still follow the trend that smaller ncSi with larger quantum confinement effects, are more effectively heated. Also from Figure 7, the GeO sample processed at 470 °C shows a significantly larger temperature increase than SiO samples, while the GeO samples processed at 510 °C and 550 °C seem to show a slightly smaller temperature increase as compared to SiO samples. This likely correspond to the larger size difference between the ncGe produced from GeO, thus the difference in phonon confinement effect is more pronounced, while the ncSi produced from SiO has a more limited difference in size.[12b] Additionally, we confirmed that the photothermal effect indeed originated from ncGe rather than the GeO_x. This was achieved by removing the GeO_x from ncGe[10] using hot water treatment of the sample processed at 470 °C (procedure described in Supporting Information). The particles are partially sintered into small aggregates and

exhibit some twinning (which commonly exists in ncGe[29]), shown in the transmission electron microscope (TEM) image in Figure 8. The energy-dispersive X-ray (EDX) spectrum (Figure S7) of a number of aggregates is dominated by the Ge

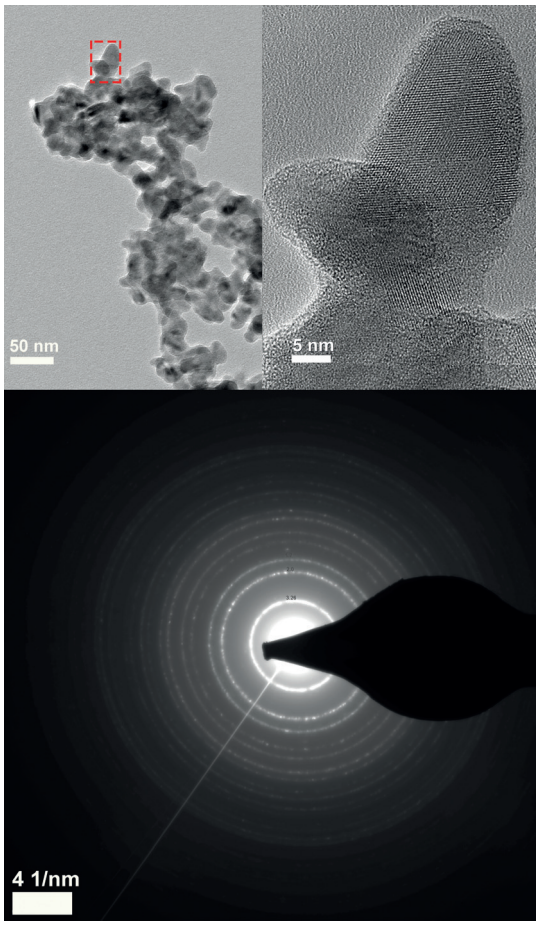

Figure 8. TEM analysis of the freestanding ncGe. Top left: BF-TEM image, Top right: HRTEM image. Bottom: SAED pattern.

signal, with the common C, O, Si, and Cu background signals from the TEM grid. However, the oxygen intensity is slight increased indicating some surface oxidation of the ncGe. The main lattice spacings in selected area electron diffraction (SAED) correspond to 3.26, 2.0, and 1.7 Å, in good agreement with crystalline Ge. The Raman analysis has also demonstrated the photothermal effect of such ncGe after the GeO_x is removed, as the temperature of the free-standing ncGe sample at 8.75 mW is also estimated to be around 1460 K (Supporting Information).

Finally, we also demonstrated the photothermal effect of ncGe in GeO under mostly visible light by illuminating a flat plastic disk of powder with a Xenon lamp (Figure S8). We selected the 470 °C sample that responded most sensitively with the Raman laser excitation for this demonstration. Shown in Table 3, within an astonishingly short time of 1 minute, the surface temperature could reach approximately 69 °C, and was around 50 °C after 30 s cooling in the air flow of a fume hood. By contrast, without the sample, the sample

Table 3: Temperature rise of the sample processed at 470 °C upon illumination with Xenon lamp for different times.

Time	Initial temp. [°C]	Light off[a] [°C]	30 s after off [°C]
1 min	27.4	ca. 69	50
2 min	28.9	ca. 97	70
5 min	29.6	ca. 121	88

[a] The surface temperature decreases rapidly upon contact with air in the fume-hood.

holder only rose to about 36 °C under the same conditions. With slightly increased time of illumination, the surface of the sample could rise to about 121 °C, well above the boiling point of water. We noticed the plastic holder that contacted with the sample melted and deformed after 5 minutes.

In conclusion, this study has presented an in-depth study of the formation of size-tunable germanium nanocrystals formed by thermal disproportionation of GeO. A processing temperature of 470 °C is effective for producing significant quantities of ncGe. The size and yield of ncGe reached a plateau at 550 °C. The impressive photothermal effect displayed by ncGe and its demonstrated size-dependence, augers well for its utility in photo-therapy, photo-desalination, and photo-catalysis.

Acknowledgements

G.A.O. is a Government of Canada Research Chair in Materials Chemistry and Nanochemistry. Financial support for this work was provided by the Ontario Ministry of Research Innovation (MRI); Ministry of Economic Development, Employment and Infrastructure (MEDI); Ministry of the Environment and Climate Change; Connaught Innovation Fund; Connaught Global Challenge Fund; Natural Sciences and Engineering Research Council of Canada (NSERC). C.Q., W.S. thank the Connaught Foundation for graduate scholarships to support their doctoral research. We thank Dr. Srebri Petrov for PXRD analysis. Microscopy support from the Karlsruhe Nano Micro Facility (KNMF) is deeply appreciated. We thank the Ontario Centre for the Characterization of Advanced Materials (OCCAM) for access to state-of-the-art surface analytical equipment.

Conflict of interest

The authors declare no conflict of interest.

Keywords: germanium monoxide · nanocrystals · nanochemistry · photothermal effect · solid-state synthesis

How to cite: *Angew. Chem. Int. Ed.* **2017**, *56*, 6329–6334
Angew. Chem. **2017**, *129*, 6426–6431

[1] P. R. Abel, A. M. Chockla, Y.-M. Lin, V. C. Holmberg, J. T. Harris, B. A. Korgel, A. Heller, C. B. Mullins, *ACS Nano* **2013**, *7*, 2249–2257.

[2] a) N. Shirahata, D. Hirakawa, Y. Masuda, Y. Sakka, *Langmuir* **2013**, *29*, 7401 – 7410; b) Z. C. Holman, U. R. Kortshagen, *Langmuir* **2009**, *25*, 11883 – 11889.
[3] T. N. Lambert, N. L. Andrews, H. Gerung, T. J. Boyle, J. M. Oliver, B. S. Wilson, S. M. Han, *Small* **2007**, *3*, 691 – 699.
[4] a) J. A. Kelly, E. J. Henderson, J. G. C. Veinot, *Chem. Commun.* **2010**, *46*, 8704 – 8718; b) M. Kanoun, C. Busseret, A. Poncet, A. Souifi, T. Baron, E. Gautier, *Solid-State Electron.* **2006**, *50*, 1310 – 1314.
[5] a) J. Hwang, C. Jo, M. G. Kim, J. Chun, E. Lim, S. Kim, S. Jeong, Y. Kim, J. Lee, *ACS Nano* **2015**, *9*, 5299 – 5309; b) W. Luo, D. Shen, R. Zhang, B. Zhang, Y. Wang, S. X. Dou, H. K. Liu, J. Yang, *Adv. Funct. Mater.* **2016**, *26*, 7800 – 7806.
[6] a) R. Gresback, Z. Holman, U. Kortshagen, *Appl. Phys. Lett.* **2007**, *91*, 093119; b) X. D. Pi, U. Kortshagen, *Nanotechnology* **2009**, *20*, 295602.
[7] B. R. Taylor, S. M. Kauzlarich, H. W. H. Lee, G. R. Delgado, *Chem. Mater.* **1998**, *10*, 22 – 24.
[8] a) X. Lu, B. A. Korgel, K. P. Johnston, *Chem. Mater.* **2005**, *17*, 6479 – 6485; b) S. Prabakar, A. Shiohara, S. Hanada, K. Fujioka, K. Yamamoto, R. D. Tilley, *Chem. Mater.* **2010**, *22*, 482 – 486.
[9] M. Hoffman, J. G. C. Veinot, *Chem. Mater.* **2012**, *24*, 1283 – 1291.
[10] E. J. Henderson, C. M. Hessel, J. G. C. Veinot, *J. Am. Chem. Soc.* **2008**, *130*, 3624 – 3632.
[11] a) C. M. Hessel, E. J. Henderson, J. G. C. Veinot, *Chem. Mater.* **2006**, *18*, 6139 – 6146; b) E. J. Henderson, J. A. Kelly, J. G. C. Veinot, *Chem. Mater.* **2009**, *21*, 5426 – 5434.
[12] a) W. Sun, C. Qian, X. S. Cui, L. Wang, M. Wei, G. Casillas, A. S. Helmy, G. A. Ozin, *Nanoscale* **2016**, *8*, 3678 – 3684; b) W. Sun, C. Qian, L. Wang, M. Wei, M. L. Mastronardi, G. Casillas, J. Breu, G. A. Ozin, *Adv. Mater.* **2015**, *27*, 746 – 749.
[13] Y. Pauleau, J.-C. Remy, *J. Less-Common Met.* **1975**, *42*, 199 – 208.
[14] D. J. Yang, W. L. Jolly, A. O'Keefe, *Inorg. Chem.* **1977**, *16*, 2980 – 2982.
[15] O. A. Babich, M. C. Ghosh, E. S. Gould, *Chem. Commun.* **2000**, 907 – 908.
[16] K. H. Gayer, O. T. Zajicek, *J. Inorg. Nucl. Chem.* **1964**, *26*, 2123 – 2125.
[17] E. J. Henderson, C. M. Hessel, R. G. Cavell, J. G. C. Veinot, *Chem. Mater.* **2010**, *22*, 2653 – 2661.
[18] A. Hohl, T. Wieder, P. A. van Aken, T. E. Weirich, G. Denninger, M. Vidal, S. Oswald, C. Deneke, J. Mayer, H. Fuess, *J. Non-Cryst. Solids* **2003**, *320*, 255 – 280.
[19] E. Gorokhov, A. Komonov, K. Astankova, GeO2 films with Ge-nanoclusters in layered compositions: structural modifications with laser pulses, INTECH Open Access Publisher, **2012**.
[20] T. M. Gross, M. Tomozawa, *J. Non-Cryst. Solids* **2007**, *353*, 4762 – 4766.
[21] C. M. Yang, H. A. Atwater, *Appl. Phys. Lett.* **1996**, *68*, 3392 – 3394.
[22] W. Sun, C. Qian, L. He, K. K. Ghuman, A. P. Y. Wong, J. Jia, A. A. Jelle, P. G. O'Brien, L. M. Reyes, T. E. Wood, A. S. Helmy, C. A. Mims, C. V. Singh, G. A. Ozin, *Nat. Commun.* **2016**, *7*, 12553.
[23] Y. Jie, A. T. S. Wee, C. H. A. Huan, Z. X. Shen, W. K. Choi, *J. Appl. Phys.* **2011**, *109*, 033107.
[24] E. Bustarret, M. A. Hachicha, M. Brunel, *Appl. Phys. Lett.* **1988**, *52*, 1675 – 1677.
[25] a) R. Gupta, Q. Xiong, C. K. Adu, U. J. Kim, P. C. Eklund, *Nano Lett.* **2003**, *3*, 627 – 631; b) G. Viera, S. Huet, L. Boufendi, *J. Appl. Phys.* **2001**, *90*, 4175.
[26] R. Jalilian, G. U. Sumanasekera, H. Chandrasekharan, M. K. Sunkara, *Phys. Rev. B* **2006**, *74*, 155421.
[27] a) S. D. Rassat, E. J. Davis, *Appl. Spectrosc.* **1994**, *48*, 1498 – 1505; b) M. Baibarac, A. Matea, M. Ilie, I. Baltog, A. Magrez, *Anal. Methods Uk* **2015**, *7*, 6225 – 6230.
[28] J. Jia, P. G. O'Brien, L. He, Q. Qiao, T. Fei, L. M. Reyes, T. E. Burrow, Y. Dong, K. Liao, M. Varela, S. J. Pennycook, M. Hmadeh, A. S. Helmy, N. P. Kherani, D. D. Perovic, G. A. Ozin, *Adv. Sci.* **2016**, *3*, 1600189.
[29] a) T. Yu, X. Pi, Z. Ni, H. Zhang, D. Yang, *Aip Adv.* **2015**, *5*, 037140; b) W. Yuan, T. Masaki, F. Kazuo, *Jpn. J. Appl. Phys.* **1999**, *38*, 7241.

Manuscript received: February 6, 2017
Final Article published: April 10, 2017

